

MMW Imaging using polarimetric measurements

Claire Migliaccio^{#1}, Laurent Brochier^{#2}, Jérôme Lanteri^{#3}, Paul Lauga^{*4}, Julien Marot^{*5}, Bruno Cosson^{**6}

[#]Université Côte d'Azur, CNRS, LEAT, France

^{*}Inst. Fresnel, CNRS, Centrale Marseille, Aix Marseille Univ.

^{**}BOWEN-ERTE, France

{¹Claire.Migliaccio, ²Laurent.Brochier, ³Jerome.Lanteri}@univ-cotedazur.fr, {⁴paul.lauga, ⁵julien.marot}@fresnel.fr

⁶bruno.cosson@bowenfr.com

Abstract — In this paper we present a complete process that goes from measurements to image extraction with the objective to help radar designers to set their system specifications. We focus on objects of interest for security scanners and therefore choose to perform the tests on a ceramic knife and a fake gun made of aluminum. We highlight polarization issues. We show that polarization has a dramatic influence on the image contrast when objects are concealed due to the creases of the clothes. This can be overcome with the use of a dual polarized system and segmentation algorithms exploiting polarizations results.

Keywords — Millimeter wave imaging, segmentation, local thresholding.

I. INTRODUCTION

The number of millimeter waves systems (MMW) for civilian security is growing rapidly. Significant advances in circuit integration, together with the short wavelength, enable the development of compact, low-cost and high-resolution systems, which are operated in an extensive set of applications such as automotive radars [1], pilot assistance for helicopters [2], Foreign Object Debris (FODs) detection on airport runways [3], and MMW scanners for detection of concealed objects [4-11].

Nevertheless, scattering properties at MMW remain relatively unknown compared to lower frequency bands. Electromagnetic modeling and measurements provide a comprehensive knowledge of scattering properties and/or Radar Cross Section (RCS). Both approaches are challenging at MMW. Modeling is complex because targets can rapidly become large compared to the wavelength, which causes simulation problems. Measurements are not easy, because the small wavelength reinforces the noise of RF electronics and the effect of alignment errors [12].

The study of scattering properties provides a set of important information for radar designers:

- Most significant scattering directions and blind areas.
- Relative levels of scattering with respect to incidence and observation.
- Sensitivity to polarization.
- Effectiveness of post-processing algorithms.

In this paper we present a complete process that goes from measurements to image extraction with the objective to help

radar designers to set their system specifications. We focus on objects of interest for security scanners and therefore perform the tests on a ceramic knife and a fake gun made of aluminum. We choose to highlight polarization issues.

Section II deals with measurements settings and the first processing stage, while section III describes the segmentation process.

II. SETTINGS AND FIRST PROCESSING STAGE

A. 3D-Scanner and measurement settings

We use the 3D-scanner installed in our laboratory [13]. Originally designed for antenna testing, the scanner is also suitable for scattering measurements as described in Fig. 1. The object under test (OUT) is on a tower made in Rohacell to minimize EM interferences. The scanner operates in W-band [75-110 GHz] but we limit ourselves to 94 GHz, which is one of the most widespread frequencies for MMW scanners [6,8,10]. We perform monostatic measurements. A standard gain horn is moving around the object with a spherical trajectory, the object being placed on a Rohacell tower centred with respect to the scan. We commute the polarization of the probe antenna (from HH to VV) with an additional motor installed on the moving arm. The scanner is linked to a PNAX that delivers amplitude and phase for every measurement point. Note that the horizontal plane is xOz while Oy is the vertical axis.

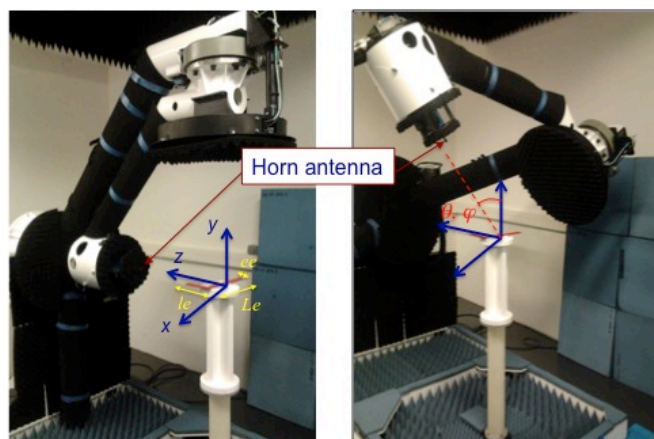


Fig. 1. 3D scanner with OUT (metallic square) for two positions of the probe antenna (standard gain horn) and definition of coordinate systems.

The geometrical scan is performed above the object and ranges from 75° to 105° in θ and φ (scan size: $30^\circ \times 30^\circ$). The scan step is 0.2° . We measure HH- and VV- polarizations. The distance between the probe antenna and the object is 585mm, which remains within the far-field zone of the horn antenna at the operating frequency. The transmitted power is defined by the standard PNA-X configuration in W-band and does not exceed 0 dBm.

B. First stage processing

In radar application such as security scanners, the end-user needs a radar image, which enables him to decide whether the object is harmless or potentially harmful. We investigate the possibility to form a flat 2D image with the back-propagation algorithm (BPA) according to equation (1):

$$A(P_i) = \sum_{\theta} \sum_{\varphi} \frac{1}{\sqrt{2d_{P_i,R}}} M(\theta, \varphi) e^{j \frac{4\pi d_{P_i,R}}{\lambda}} \quad (1)$$

Where:

- P_i is the centre of the i^{th} pixel in the image.
- $M(\theta, \varphi)$ is the measured complex value of electric field with respect to the receivers position defined by (θ, φ) .
- $d_{P_i,R}$ is the distance between receiver and point P_i .
- λ is the free space wavelength.

Finally, from a theoretical point of view, the expression of $A(P_i)$ is valid when the object is in the far field of the radar system, which is the case with our settings.

The observation plane where we form the image is 5 mm above the object (Fig. 2). The scanner is in semi-anechoic environment (Fig. 1). We intentionally kept interferences coming from the surrounding for increase the overall noise level because we want to investigate the disturbance caused by the noise in the reconstruction of the object. Figure 2 shows the 3D scan and the reconstruction plane, the object (OUT) being placed at $y=0$.

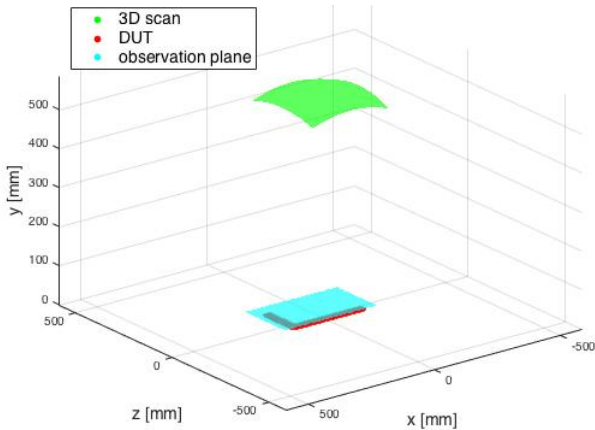


Fig. 2. 3D view of the scan range with OUT and observation plane.

The 2D image (instead of a 3D one) is relevant in MMW security scanners because we take advantage of the

intrinsically high lateral resolution due to the short wavelength. Moreover, objects are generally placed on the front or at the back of the torso that can be seen as a flat surface in a first approximation. Finally, in security scanners the system will be tuned for scanning within a predetermined range, which means that we know in advance at which distances we need to form the images. In this case, we don't need resolution in depth, *i.e.* range resolution, and we can replace wideband measurements by a CW one. This significantly improves the signal to noise ratio (SNR) because of the limited bandwidth.

C. Results

Figures 4 to 6 show the images obtained with BPA for the various objects taken from measurements in HH- and VV- polarizations at 94 GHz. For getting closer to the final application, we have also concealed the fake gun under a leather jacket (Fig. 3). We intentionally chose a thick jacket (3 mm) to reinforce the attenuation. We want to test if weak reflected signals still provide workable images.



Fig. 3. Left: fake gun. Right: concealed by a leather jacket.

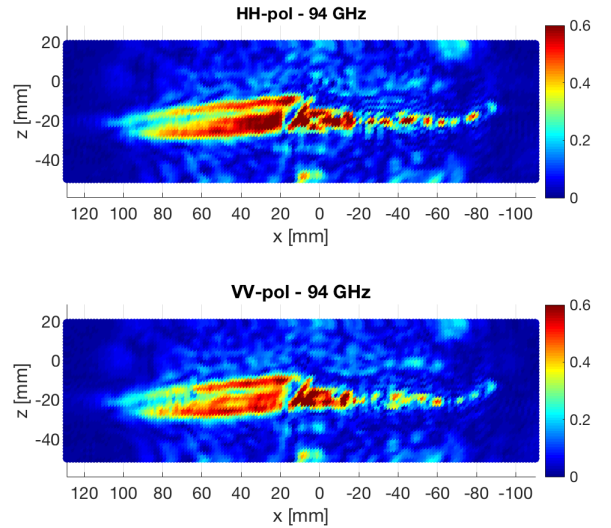


Fig. 4. Images of the ceramic knife obtained with BPA.

Except for the amplitude level, which is higher in HH, the sensitivity to polarization is low for non-concealed objects. This was expected due to the generally large electrical dimensions of OUTs at MMW. In this case, the number of preferential directions "seen by the wave" decrease and the OUT is finally seen the same way in both polarizations. Note that the difference in the received amplitude level might be due to the influence of the additional rotation stage used in the

scanner rather than to the OUT's response. This has to be further investigated.

On the contrary, results are better in vertical polarization when the gun is concealed. This is due to the creases of the leather jacket. This shows the importance of polarimetric measurements. The creases of clothes cannot be predicted. We see that for thick clothes they cause significant attenuation depending on the investigated polarization. To overcome this difficulty, we recommend including both polarizations in the final system and to develop algorithms to extract the object features from images adapted to low and/or high contrasts. Of course this will also increase the system complexity and cost. The final choice shall be left to radar designers.

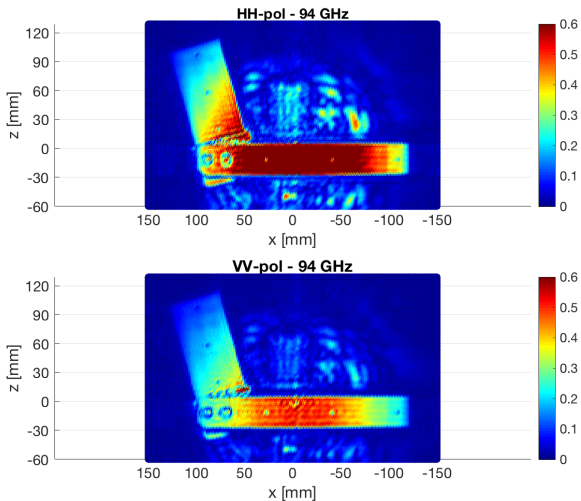


Fig. 5. Images of the fake gun obtained with BPA.

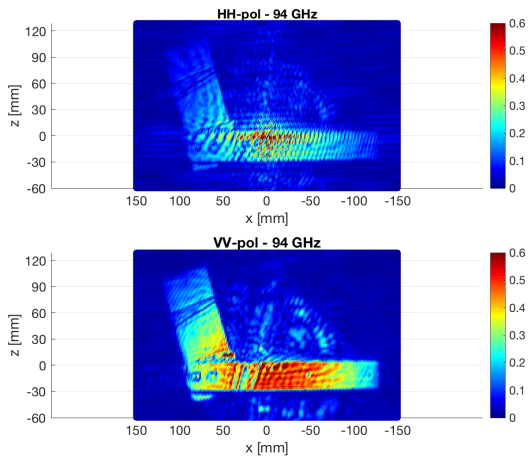


Fig. 6. Images of the fake gun concealed by a leather jacket (5mm thickness) obtained with BPA.

The shape of the objects is recognizable on all images. However, in spite of the theoretical transparency of the Rohacell material used for the tower that supports the OUT, the circular shape of the Rohacell tower is particularly visible on Fig. 5 and causes a significant level of noise. Therefore, a

simple threshold is not adequate to preserve the shape of the object of interest. Hence, we adapt a segmentation method.

III. SEGMENTATION

The proposed segmentation method falls into three steps: Firstly, we apply low pass filtering to remove the unexpected noise. Secondly, we use an adaptive Niblack thresholding [14], which applies local thresholding, considering the local values of mean and standard deviation of the grey levels. The Niblack method includes a parameter k , which emphasizes the influence of the standard deviation in the value of the threshold. In the experiments presented below, parameter k is set empirically to 0.22 for the fake gun, and to 0.44 for the knife. Thirdly, we apply a mathematical morphology operator [15]. This operator is the combination of an erosion with a square structuring element to remove part of the unexpected features which are remaining in the threshold image and a dilation with a structuring element whose shape depends on the considered object: we use a square and a line when fake guns and knives are respectively considered.

The proposed method is exemplified on an image of ceramic knife (Fig. 7), and a concealed fake gun (Fig. 9 for the final segmentation result obtained with H and V polarization).

Note that the pixels of the final images are Boolean after step (d) whatever the initial contrast of the BPA image was. Once information is detected the pixel's intensity is the same even for initially weak responses of the object, *i.e.* for the concealed fake gun in HH-polarization. We will take advantage of this Boolean property to easily combine images.

We decided to present the results associated with the concealed gun because the difference in the segmentation result is even more dramatic than with the gun that is not concealed.

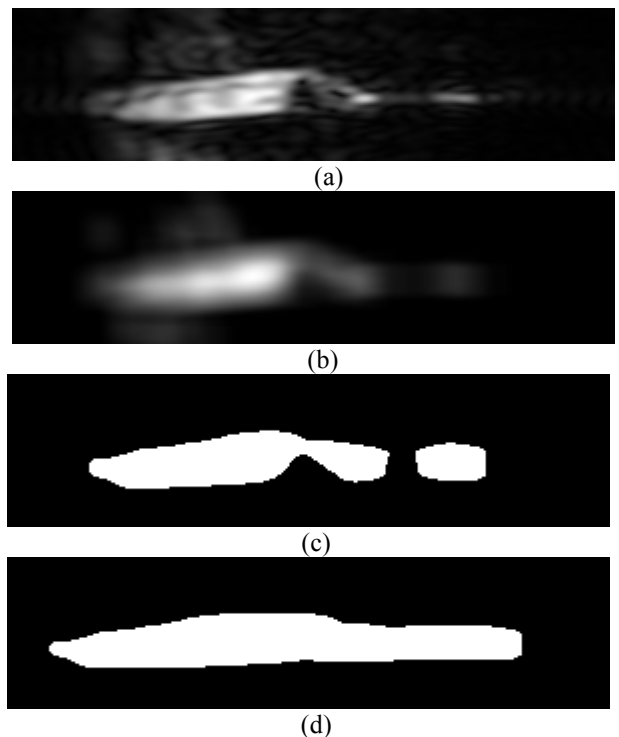


Fig. 7. Knife: (a) Processed image; (b) Low pass filter; (c) Segmentation; (d) Mathematical morphology

We notice that, depending on the considered object, some unexpected features may remain in the final segmented image (image (d)). The largest non-disrupted object can then be selected for further processing, for instance object identification. As expected, a significant difference exists between the segmentation result obtained with the H polarization and the V polarization. In Fig. 9, we present the combination of the final segmentation result obtained from H and V polarization. Indeed, these two segmentation results are complementary. Hence, to combine both images, we simply make a Boolean summation (“OR” gate).

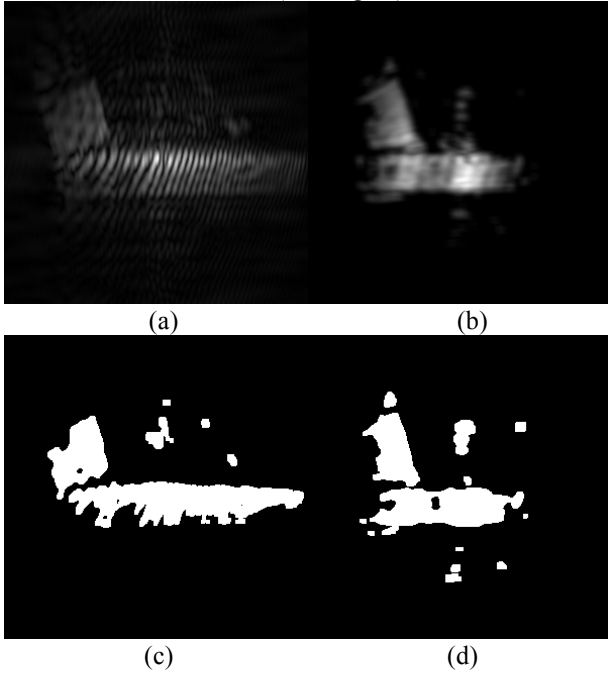


Fig. 8. Fake gun concealed by a leather jacket: (a) H polarization: Processed image; (b) V polarization: Processed image; (c) H polarization: Mathematical morphology; (d) V polarization: Mathematical morphology



Fig. 9. Fake gun concealed by a leather jacket: combination of the result obtained with combined H and V polarizations

IV. CONCLUSION

In this paper we have investigated the influence of polarization on images obtained from monostatic measurements at 94 GHz. The objective is to help radar

designers to settle their system specifications. We focus on the detection of concealed objects. We show that polarization has a dramatic influence on the image contrast when objects are concealed due to the creases of the clothes. This can be overcome with the use of a dual polarized system and segmentation algorithms exploiting polarizations results.

In a future work, we aim at performing classification of radar images with a machine learning algorithm such as support vector machines.

ACKNOWLEDGMENT

Authors would like to thank the French BPI (*Banque Publique d'Investissement*) and the *Région PACA* (Provence Alpes Côte d'Azur) for supporting the *FUI-Scanvision* project.

REFERENCES

- [1] G. M. Rebeiz et al., “RF-Beamforming Phased-Arrays with Imaging Capabilities for Next-Generation Automotive Radar,” 2015 IEEE-MTT ICMIM, Heidelberg, Germany, 27-29 April 2015.
- [2] C. Migliaccio, B. D. Nguyen, Ch. Pichot, N. Yonemoto, K. Yamamoto, K. Yamada, H. Yasui, W. Mayer, A. Gronau, and W. Menzel, “Millimetre Wave Radar for Rescue Helicopters,” 9th International Conference on Control, Automotion, Robotics and Vision (ICARV 2006), WA6, p. 29, Singapore, 5-8 December 2006.
- [3] S.P. Beasley, G. Binns, R. Hodges, and R.J. Badley, “Tarsier, a Millimetre Wave Radar for Airport Runway Debris Detection,” Proc. EURAD’04, Amsterdam, 2004.
- [4] D. M., D. L. McMakin, and T. E. Hall, “Three-dimensional millimeter-wave imaging for concealed weapon detection,” IEEE-MTT, vol. 49, no. 9, pp. 1581-1592, 2001.
- [5] N. A. Salmon *et al.*, “An all electronic passive millimetre wave imaging system,” in Proceedings of SPIE, Vol. 5789, Passive Millimeter-Wave Imaging Technology VII, Defense and Security, 2005, Orlando, Florida, United States.
- [6] T. D. Williams, N. M. Vaidya, “A compact low-cost, passive MMW security scanner,” in Proceedings of SPIE, Vol. 5789, Passive Millimeter-Wave Imaging Technology VII, Defense and Security, 2005, Orlando, Florida, United States.
- [7] S. S. Ahmed, A. Schliessel and P.L Schmidt, “A Novel Fully Electronic Active Real-Time Imager Based on a Planar Multistatic Sparse Array,” IEEE-MTT, vol. 59, no. 12, pp. 3567-3576, Dec. 2011.
- [8] N.A. Salmon, “3D Radiometric Aperture Synthesis Imaging,” IEEE - MTT, vol.63, no.11, pp.3579–3587, Nov.2015.
- [9] O.Yurduseven, J.N.Gollub, A.Rose, D.L.Marks, and D.R.Smith, “Design and Simulation of a Frequency-Diverse Aperture for Imaging of Human-Scale Targets,” IEEE Access (Volume: 4), pp.5436-5451, August 2016.
- [10] <http://www.millivision.com>, see Millivision’s Portal System S350.
- [11] <https://www.mc2-technologies.com/mm-imager/>
- [12] F. Nsengiyumva *et al.*, “New W-Band Scattering Measurement System: Proof of Concept and Results for 2-D Objects,” IEEE-TAP 66 (12), Dec. 2018, pp. 7224 - 7236.
- [13] F. Ferrero, Y. Benoit, L. Brochier, J. Lanteri, J-Y Dauvignac, C. Migliaccio and S. Gregson, “Spherical Scanning Measurement Challenge for Future Millimeter Wave Applications,” AMTA 2015, AMTA 37th Annual Meeting & Symposium Long Beach, California, Oct 11 – 16, 2015.
- [14] Khurshid, K., Siddiqi, I., Faure, C., & Vincent, N. (2009, January). Comparison of Niblack inspired Binarization methods for ancient documents. In *Document Recognition and Retrieval XVI* (Vol. 7247, p. 72470U). International Society for Optics and Photonics.
- [15] Sghaier, Moslem Ouled, Samuel Foucher, and Richard Lepage. "River extraction from high-resolution sar images combining a structural feature set and mathematical morphology." *IEEE Journal of Selected Topics in Applied Earth Observations and Remote Sensing* 10.3 (2017): 1025-1038.